Photodissociation of gas phase I_3^- using femtosecond photoelectron spectroscopy

Martin T. Zanni, B. Jefferys Greenblatt,[a] Alison V. Davis, and Daniel M. Neumark[b]

Department of Chemistry, University of California, Berkeley, California 94720
and Chemical Sciences Division, Lawrence Berkeley National Laboratory, Berkeley, California 94720

The photodissociation dynamics of gas phase I_3^- following 390 nm excitation are studied using femtosecond photoelectron spectroscopy. Both I^- and I_2^- photofragments are observed; the I_2^- exhibits coherent oscillations with a period of 550 fs corresponding to ~ 0.70 eV of vibrational excitation. The oscillations dephase by 4 ps and rephase at 45 and 90.5 ps on the anharmonic I_2^- potential. The gas phase frequency of ground state I_3^- is determined from oscillations in the photoelectron spectrum induced by resonance impulsive stimulated Raman scattering. The dynamics of this reaction are modeled using one- and two-dimensional wave packet simulations from which we attribute the formation of I^- to three-body dissociation along the symmetric stretching coordinate of the excited anion potential. The photodissociation dynamics of gas phase I_3^- differ considerably from those observed previously in solution both in terms of the I_2^- vibrational distribution and the production of I^-. © *1999 American Institute of Physics.* [S0021-9606(99)01930-3]

I. INTRODUCTION

Chemical reactions in the gas phase can now be probed by an impressive arsenal of frequency and time-resolved methods, leading to a detailed characterization of asymptotic product distributions and short-time transition state dynamics. It is of considerable interest to understand how the dynamics of even the simplest of chemical reactions is altered when the reaction is initiated in a liquid. The reaction coordinate near the transition state can be modified significantly for reactions in liquids,[1] and solvent friction near the transition state can also play an important role.[2] The rapid relaxation processes that occur in liquids have hindered the comparison of gas and liquid phase reaction dynamics. However, the development of ultrafast pump–probe laser techniques now enables one to initiate reactions and probe the products on a sub-100 fs time scale, thereby in principle yielding nearly nascent product distributions that can be compared to gas phase results.

Thus far, only one comparison of this type has been made for a reaction yielding molecular products, namely, the photodissociation reaction $HgI_2 \rightarrow HgI + I$, which was studied in the gas phase and in ethanol by Zewail and co-workers[3–6] and by Hochstrasser and co-workers,[7–10] respectively. During the last few years, a series of femtosecond time-resolved experiments on the photodissociation of I_3^- in ethanol solution have been performed in the laboratories of Ruhman and co-workers[11–16] and, more recently, by Vohringer and co-workers[17–19] that have yielded the vibrational distribution of the I_2^- photoproduct within a few hundred fs of the photodissociation pulse through the observation of vibrational

coherences. However, until very recently,[20,21] no gas phase data were available for this reaction. In this article, we report a gas phase photodissociation study of the I_3^- anion using femtosecond photoelectron spectroscopy (FPES) which allows a direct comparison with the liquid phase results.

The spectroscopy and dynamics of I_3^- have been studied extensively in solution. Its absorption spectrum consists of two broad bands centered at 360 and 290 nm.[22–28] The spectral assignment of these bands has been somewhat controversial,[23–25] although the solution phase work has shown that excitation into either band results in dissociation to ground state I_2^- anions.[12,17] The resonance Raman spectrum of I_3^- reveals a long progression of the symmetric stretch,[26,27,29] indicating that at least the initial motion on the excited state is along this coordinate. However, some intensity in the antisymmetric stretch was also seen; this has been attributed to symmetry breaking of the linear triatomic by the solvent.[29,30]

In the work most relevant to that presented here, Banin *et al.*[12,13] performed femtosecond transient absorption spectroscopy measurements on I_3^- in ethanol, in which the anion was excited at 308 nm and the resulting time-dependent absorption was monitored at a series of wavelengths. They observed coherently vibrating I_2^- anions in their $\tilde{X}\,^2\Sigma_u^+$ state as early as 500 fs after the initial excitation. At this time the I_2^- products are in an average vibrational state of $\langle v \rangle = 12$, and the coherent motion is irreversibly lost within 4 ps due to interactions with the solvent molecules. Coherences due to ground state I_3^- were also observed with a frequency of 111 cm^{-1} and attributed to excitation via resonance impulsive stimulated Raman scattering (RISRS). No evidence for I^- production was seen, even though dissociation to $I^- + I_2$ is energetically favored with respect to $I_2^- + I$ by ~ 0.6 eV. More recently, Kühne and Vöhringer have performed similar ex-

periments involving excitation of the lower band at 400 nm (Refs. 17 and 18) and the blue edge of the upper band at 266 nm.[19] They also observed coherences due to vibrationally excited I_2^- products ($\langle v \rangle = 12$) and oscillating I_3^- parent molecules. In addition, their work at 266 nm showed indirect evidence for I^- photoproducts with a 20% yield.

Only a few studies of gas phase I_3^- have been performed. Do *et al.*[20] have measured the bond strength of ground state I_3^- through collision-induced dissociation in a tandem mass spectrometer, obtaining a value of 1.31 ± 0.06 eV for dissociation to $I_2 + I^-$ products. This is 300 meV larger than previously reported.[31] Our group has reported a preliminary investigation of I_3^- photodissociation using FPES.[21] In addition, we have measured a high resolution (8–10 meV) photoelectron spectrum of I_3^-,[32] as well as the photofragment kinetic energy release from I_3^- photodissociation at a series of wavelengths.[33]

In this study, FPES was used to study the photodissociation dynamics of gas phase I_3^- following excitation of the lower absorption band at 390 nm, thereby allowing a detailed comparison between the gas and condensed phase dynamics. In the FPES experiment, I_3^- is electronically excited with a femtosecond pump pulse. The resulting nonstationary state is photodetached by a femtosecond probe pulse and the photoelectron spectrum is measured. By performing this experiment at a series of pump–probe delay times one obtains a progression of snapshots detailing the dynamics induced by the pump pulse. As in the solution phase experiments, we observe coherently vibrating I_3^- anions caused by a RISRS process as well as coherent, vibrationally excited I_2^- photoproducts. The I_2^- vibrational distribution, however, is centered at significantly higher vibrational levels than in solution and exhibits rephasing dynamics. We also observe the formation of the I^- product, which was not seen in the condensed phase studies at 308 and 400 nm.

II. EXPERIMENT

The FPES experiment consists of two major components: a negative ion photoelectron spectrometer with high collection efficiency and a high repetition rate femtosecond laser. Each has been described in detail elsewhere[34,35] and will only be briefly described below.

The photoelectron spectrometer, Fig. 1, is designed to be compatible with the high laser repetition rate and the low photoelectron signal expected for a two-photon pump–probe experiment. Argon carrier gas (10 psig) is passed over crystalline I_2 and supersonically expanded through a pulsed piezoelectric valve operating at a 500 Hz repetition rate. Anions are generated by a 1 keV electron beam which crosses the expansion just downstream of the nozzle, and are injected into a Wiley–McLaren time-of-flight mass spectrometer by applying pulsed extraction and acceleration fields perpendicular to the molecular beam axis. After passing through several differentially pumped regions, the ions enter the detector chamber and interact with the pump and probe pulses. The ions can either be monitored with a retractable, in-line microchannel plate detector or with a second, off-axis reflectron/microchannel plate assembly to record the photo-
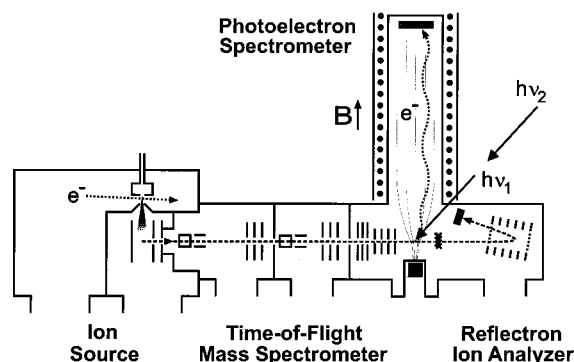
FIG. 1. Schematic of the apparatus showing the ion source region, time-of-flight mass spectrometer, photofragment reflection assembly, and magnetic bottle photoelectron time-of-flight spectrometer.

fragment mass spectrum. High electron collection efficiency is achieved with a ''magnetic bottle'' time-of-flight analyzer[36] whose energy resolution has been optimized using a pulsed decelerator[37,38] applied to the ions just prior to photodetachment. The instrument resolution is approximately 30 meV for an electron kinetic energy (eKE) of 0.8 eV and degrades as ''approximately'' (eKE)$^{1/2}$.

The magnetic bottle time-of-flight analyzer is calibrated by a quadratic fit to three peaks: two at 1.76 and 0.77 eV generated by photodetachment of I^- by 260 nm light [corresponding to the $I(^2P_{3/2})$ and $I^*(^2P_{1/2})$ states, respectively], and an additional peak at 0.12 eV from photodetachment of I^- to the $I(^2P_{3/2})$ state by 390 nm light. The calibration is more accurate for electron energies below 0.5 eV than in our previous report using a two-point linear fit.[21]

The pump and probe pulses are generated by, respectively, doubling and tripling the 780 nm output of a Clark-MXR regeneratively amplified Ti:sapphire laser system. The energy of the resulting 260 nm (4.77 eV) probe pulse is 20 μJ and its duration is 130 fs full width at half maximum (FWHM) (sech^2), the latter measured by difference frequency mixing with the fundamental light at 780 nm. The pulse energy of the pump pulse at 390 nm (3.18 eV) is typically 90 μJ; this pulse is characterized by difference frequency cross correlation with the previously determined probe pulse and has a FWHM of 100 fs. The relative delay between the pump and probe pulses is adjusted with a computer controlled translation stage, and the beams are collinearly recombined and gently focused prior to entering the vacuum chamber. The probe pulse alone has sufficient energy to detach I_3^-, producing a background signal observed in the experiment. By passing the pump beam through a 250 Hz chopper (New Focus, 3501), shot-to-shot background subtraction can be performed, and the electron signal during this time is integrated and used to normalize different scans.

The vacuum chamber window affects the individual pulse widths and the relative delay between the pump and probe pulses. Two-color above-threshold detachment (ATD)[39] of I^- is used to characterize the pulses and determine the zero of time inside the chamber. The probe pulse alone produces a photoelectron spectrum with two peaks at 0.77 and 1.71 eV. When the pump and probe pulses are

J. Chem. Phys., Vol. 111, No. 7, 15 August 1999

Photodissociation of I$_3^-$ 2993
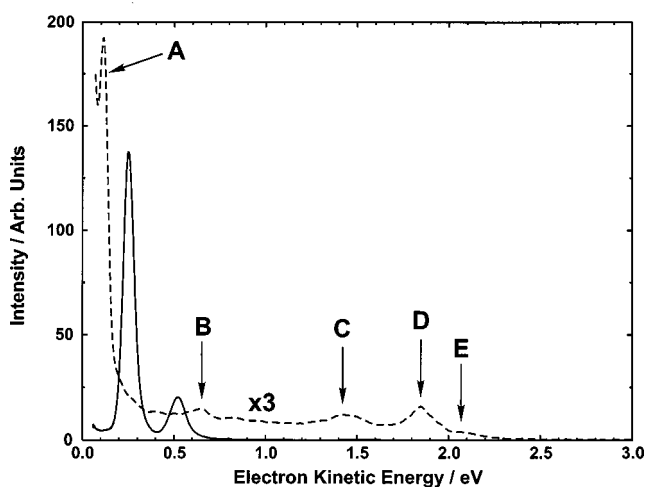
FIG. 2. One-color photoelectron spectra of I$_3^-$. Results from detachment at 260 nm probe (4.77 eV, solid line) and 390 nm (3.18 eV, dashed line) photon energy are shown.

FIG. 3. Experimental FPES spectra of I$_3^-$ from −150 to 975 fs in 75 fs steps. The scaling factors for high and low energy ranges are shown, and a base line for each delay time is marked with a dashed line. The approximate center of the broad feature between 0.8 and 1.6 eV is marked with a dot to show its time evolution. An expanded view of the high energy signal at ∼5 ps is displayed in the inset.

temporally overlapped, additional peaks are observed that correspond to shifting the I$^-$ peaks 3.18 eV toward higher eKE, i.e., the photon energy of the pump pulse. From the intensity of this two-color signal as a function of pump–probe delay, we determine the zero-delay time and the cross correlation of the pump and probe pulses inside the vacuum chamber. This yields a convoluted FWHM of 175 fs.

III. RESULTS

Here in Sec. III we present one-color photoelectron spectra of I$_3^-$ taken separately with 390 and 260 nm light. We then present measurements of the photofragment yield upon dissociation with the 390 nm pump pulse, and the time-resolved FPES spectra taken with the combined pump and probe pulses.

A. One-color photoelectron spectra

Before considering the two-photon FPES spectra, the effect of the individual pump and probe pulses on the I$_3^-$ anion needs to be determined. Shown in Fig. 2 (solid line) is the one-color photoelectron spectrum of I$_3^-$ taken at the probe wavelength, 260 nm (4.77 eV), and plotted as a function of eKE. Two broad, featureless transitions are seen, centered at 0.52 and 0.25 eV. These peaks are assigned to transitions to the ground and first excited electronic states, respectively, of neutral I$_3$. From the peak centers one obtains the vertical detachment energy (VDE) from

$$\text{VDE} = h\nu - e\text{KE}. \tag{1}$$

This yields VDEs of 4.25 and 4.52 eV for the small and large peaks, corresponding to the vertical transition energies from the anion to the two neutral electronic states. As discussed elsewhere, the peak at 0.52 eV exhibits vibrational structure at higher resolution and corresponds to a bound state of I$_3$.[32]

Also shown in Fig. 2 (dashed line) is the photoelectron spectrum measured at the pump wavelength, 390 nm. This spectrum exhibits intensity up to eKE = 2.3 eV with peaks centered at 0.12, 0.65, 1.45, 1.85, and 2.09 eV labeled

(A)–(E). The presence of features at higher eKE than in the 260 nm spectrum indicates that multiphoton processes are contributing to the 390 nm spectrum. Indeed, when $h\nu$ in Eq. (1) is taken as 6.36 eV (two 390 nm photons), the VDEs of peaks (D) and (E) match the VDEs of the two 260 nm bands. Peak (A), the most prominent peak in the 390 nm spectrum, is due to photodetachment of I$^-$ to the I($^2P_{3/2}$) state by one photon of 390 nm light. This peak must also arise from a two-photon process in which one photon dissociates the I$_3^-$ and the second photon detaches the I$^-$ photofragment. Peaks (B) and (C) at 0.65 and 1.45 eV presumably arise from two-photon photodetachment to higher lying states of neutral I$_3$.

B. Photofragment mass spectroscopy

The photoelectron spectrum at 390 nm indicates that I$^-$ is a photoproduct. To confirm this, the photofgragment mass distribution resulting from excitation of I$_3^-$ at 390 nm was determined using the reflectron assembly in our instrument (see Fig. 1). Equal yields of I$^-$ and I$_2^-$ were observed for pump powers ranging over an order of magnitude. Although the pump photon also detaches I$^-$ products, discussed in Sec. II, the relative yield between I$^-$ and I$_2^-$ does not seem to be affected. A more detailed power study was presented in our earlier report.[21]

C. Femtosecond photoelectron spectroscopy of I$_3^-$ photodissociation

Figure 3 shows successive time-resolved, two-photon photoelectron spectra for pump–probe delays of ∼150–975 fs in 75 fs increments. As was discussed in Sec. II, the background from the probe pulse (260 nm, Fig. 2) has been subtracted through the course of the experiment. Thus, at positive delay times, the background features from the probe pulse would normally be less than zero due to bleaching of the ground state. In Fig. 3, however, a constant fraction of
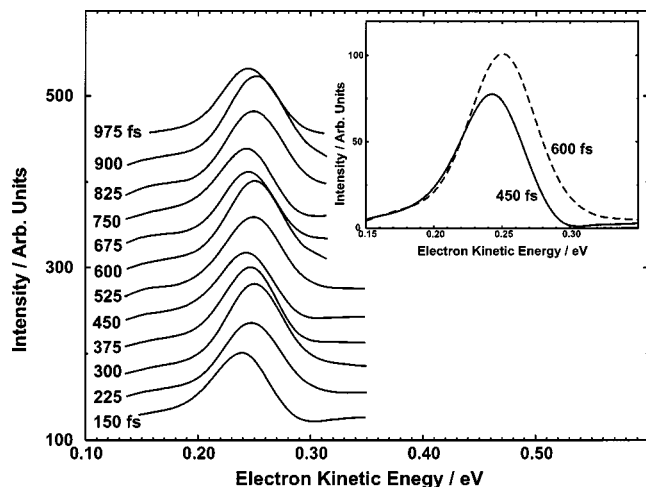
FIG. 4. Expanded view of the I_3^- feature at 0.25 eV showing oscillatory motion. The inset overlays the spectra at 450 (solid line) and 600 fs (dashed line) to illustrate the intensity change associated with this oscillation.

FIG. 5. Intensity at 0.28 eV from 5 to 30 ps in 75 fs steps. The inset displays the Fourier transform of this signal which consists of one peak at 112 ± 1 cm^{-1}.

background signal has been added back in to make the spectra positive at all delay times. Likewise, the signal arising from two-photon detachment by the pump pulse alone (390 nm, Fig. 2) has been subtracted to enhance the two-color features.

The spectra follow the same general trends we have observed before on other systems.[40,41] At -150 fs, when the probe pulse comes before the pump pulse, a signal due to detachment of the I_3^- by the probe pulse is seen (260 nm, Fig. 2). As the delay time is increased, the pump and probe pulses begin to overlap, and the two I_3^- features decrease in intensity. This is accompanied by the appearance of an electron signal at higher eKE, out to ~ 3.8 eV. Starting at 75 fs, this higher energy signal begins coalescing into two features that eventually become two tall, narrow peaks at 0.77 and 1.71 eV. The intensities of these peaks increase steadily up to about 600 fs, and are split by the spin–orbit splitting of atomic iodine. These features are due to the atomic $I(^2P_{3/2})\leftarrow I^-$ and $I^*(^2P_{1/2})\leftarrow I^-$ transitions, respectively, arising from detachment of the I^- photoproduct. Additionally, first apparent at 150 fs, there is a signal between 0.9 and 1.6 eV, and a low intensity signal out to 3.2 eV; these features are present at the longest delay times probed in our experiments. The low intensity signal from 1.8 to 3.2 eV is displayed in the inset of Fig. 3, taken at a delay time of ~ 5 ps. As will be discussed below, these features result from I_2^- photoproduct.

Overall, Fig. 3 demonstrates how FPES can provide a complete picture of a reaction occurring in real time. By performing a single measurement (i.e., photoelectron spectroscopy) at each delay time, we observe depletion of the I_3^- reactant and the accompanying evolution of the I^- and I_2^- products. We now consider these three aspects of the spectra in more detail.

1. I_3^- features

In addition to a steady drop in intensity of the two I_3^- features from -150 to 225 fs, close examination of the two bands at 0.25 and 0.52 eV reveals time-dependent oscillations. Figure 4 shows an enlarged view of the lower energy
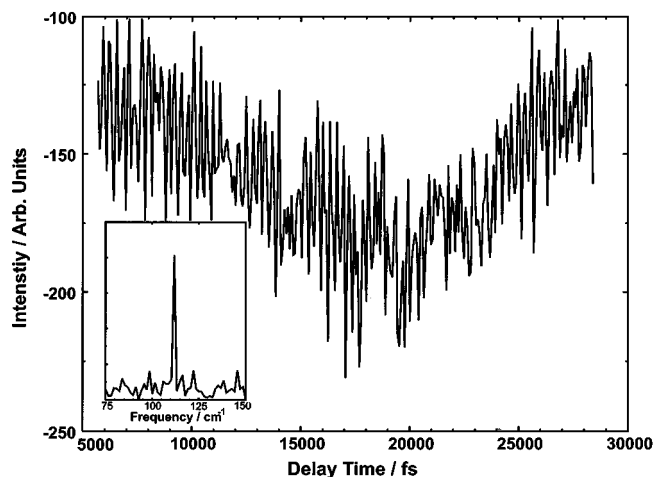
peak, the maximum of which oscillates between 0.24 and 0.25 eV with a 300 fs period. The total intensity of this band also depends on the position of the peak. The intensity is smaller when the peak is centered at low eKE and larger at high eKE; two examples are displayed in the inset of Fig. 4. The periodic nature of the oscillatory motion is seen more clearly in Fig. 5, which shows a cut through the photoelectron spectrum at 0.28 eV from 5 to 30 ps with a step size of 90 fs. This energy exhibits the largest oscillatory amplitude. The inset of Fig. 5 displays the Fourier transform of the time spectrum at 0.28 eV which is dominated by a single frequency at 112 ± 1 cm^{-1}. No higher harmonics are observed.

2. Atomic iodine features

Figure 6 shows an expanded view of the atomic $I(^2P_{3/2})\leftarrow I^-$ feature, which evolves in two distinct steps. From 150 to 300 fs, a broad band is observed with a down-
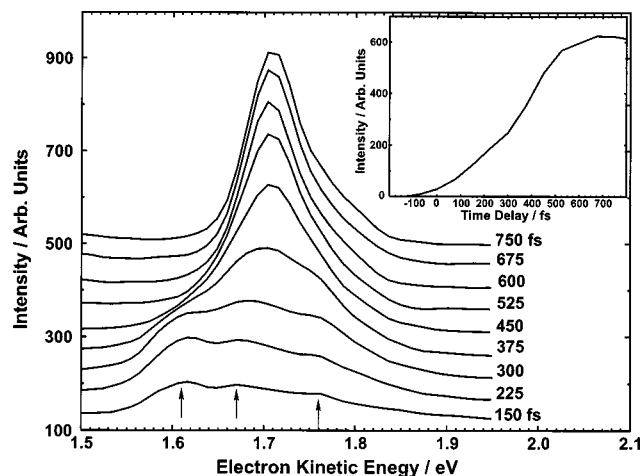
FIG. 6. Expanded view of the atomic $I(^2P_{3/2})\leftarrow I^-$ feature at 1.7 eV. The arrows indicate small features that persist for early time delays. Note the dramatic decrease in width beginning at 300 fs. In the inset, the time dependence of the signal at 1.70 eV is shown. It reaches its half maximum height by 350 fs.

J. Chem. Phys., Vol. 111, No. 7, 15 August 1999

Photodissociation of I$_3^-$ 2995
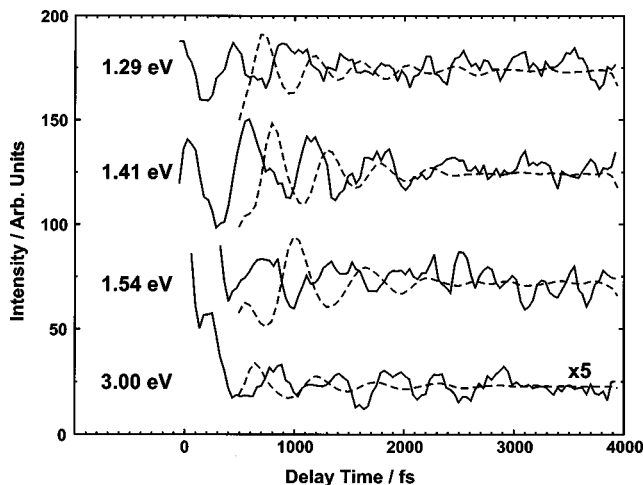
FIG. 7. Time dependent signal at several values of eKE from 0 to 4000 fs illustrating the I$_2^-$ product coherences (solid line) with ~550 fs period. Simulations (discussed in Sec. IV D) are also displayed (dashed line).

FIG. 8. Time dependent signal at from 41 to 46 ps illustrating the I$_2^-$ rephasing dynamics.

ward sloping intensity from 1.55 to 1.8 eV that exhibits small features at 1.61, 1.67, and 1.76 eV, marked with arrows. Starting at 300 fs, the entire feature becomes progressively narrower. The shoulder at 1.61 eV drops in intensity and the distribution becomes peaked at 1.71 eV. This transformation continues until approximately 600 fs after which no additional changes are observed.

In the inset of Fig. 6 a cut through the photoelectron spectrum at 1.70 eV is displayed which provides a measure of I$^-$ production as a function of time. The intensity reaches half of its maximum by 350 fs, although its full height is not reached until 600 fs. Hence, no more I$^-$ is formed after 600 fs. Since the FWHM of the convoluted pump and probe pulses is 175 fs, the formation of I$^-$ occurs long after interaction with the pump pulse has ceased. Similar behavior is seen for the I*($^2P_{1/2}$)←I$^-$ transition.

3. Intermediate energies

The electron signal between 0.9 and 1.6 eV also exhibits oscillatory motion. Discernible beginning at 150 fs with a maximum near 1.4 eV, the intensity shifts to lower eKE and back again, completing a full oscillation by approximately 825 fs. In Fig. 3, a small dot marks the approximate center of intensity at each time delay to emphasize this behavior. The oscillatory motion is shown more clearly in Fig. 7 (solid line) where slices at 1.29, 1.41, and 1.54 eV are observed with a period of approximately 550 fs (simulations are shown by dashed lines and will be discussed in Sec. IV D). The phase of the oscillations shifts with increasing energy until a 180° phase shift is observed between 1.29 and 1.54 eV. The amplitude of the oscillations also varies with energy and is largest at 1.41 eV. Note that at 1.41 eV the amplitude of the second oscillation is larger than the first. Also shown in Fig. 7 is a slice at 3.00 eV that also exhibits oscillatory motion with the same frequency. These oscillations are of lower intensity and approximately 180° phase shifted from the oscillations appearing around 1.41 eV. At all electron energies the oscillations decay by 4 ps.
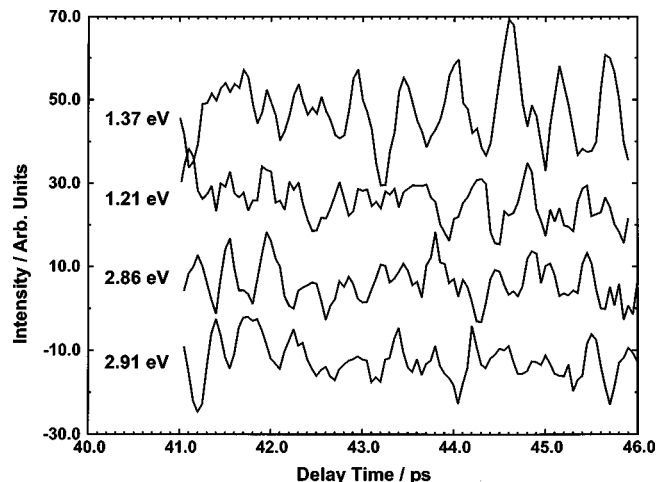
An oscillatory structure with the same period reappears at 45 and 90.5 ps. Figure 8 shows slices at 1.21, 1.37, 2.86, and 2.91 eV near 45 ps. At 1.21 and 1.37 eV, the oscillations are approximately 180° out of phase, and, likewise, the oscillations at 2.86 and 2.91 eV appear 180° out of phase, although they are centered at approximately 42 ps. At 90.5 ps, large oscillations are again observed (not shown).

IV. ANALYSIS AND DISCUSSION

In a similar fashion to that in Sec. III, the analysis and discussion proceed along three lines: analysis of the I$_3^-$ bands at 0.31 and 0.55 eV, the origin of the atomic I$^-$ features at 1.71 and 0.77 eV, and discussion of the nature of the oscillatory structure from 0.9 to 1.6 eV.

A. I$_3^-$ coherences

In the FPES experiment, the pump pulse promotes I$_3^-$ to the first excited state on which the reaction takes place. However, as was shown for I$_2^-$,[42] the pump pulse also creates a coherent superposition of vibrational levels on the ground state potential energy surface of the anion that can be detected in the time-resolved photoelectron spectra. The process by which this occurs, RISR, has been well documented in previous femtosecond absorption experiments,[43–47] including the studies of I$_3^-$ in solution.[12,17,19]

In our FPES experiment, RISRS induced by the pump pulse results in modulation of the photoelectron spectrum of the I$_3^-$ ground state. Thus, the oscillations superimposed on the peaks at 0.31 and 0.55 eV can be unambiguously assigned to coherent I$_3^-$ vibrational motion induced by the pump pulse. This point is worth emphasizing; while the frequency associated with these oscillations, 112 ± 1 cm^{-1}, is close to the I$_2^-$ fundamental at 110 cm^{-1}, the photoelectron spectrum of I$_2^-$ occurs at very different eKE values.

The 112 cm^{-1} frequency is assigned to the I$_3^-$ symmetric stretch. This value lies only 1 cm^{-1} to the blue of the solution phase resonance Raman value.[27,48] However, in solution the RISRS oscillations associated with I$_3^-$ decay in approximately 3 ps due to interactions with the solvent molecules.

Such interactions are obviously absent in the gas phase and the oscillations are seen to persist indefinitely.

B. I⁻ photofragments

Our finding of a 50% yield for I^- products based on reflection measurements is of interest since the formation of atomic I^- was not observed in the solution phase work at 400 and 308 nm.[12,17] However, direct observation of I^- in solution is difficult since it is a closed-shell species with no low-lying electronic states. In the solution phase studies by Vöhringer and co-workers[19] and by Banin and Ruhman,[12] the amount of I^- production was indirectly determined at delay times longer than 10 ps. These studies indicate that, at 400 and 308 nm, 100% of the dissociated I_3^- has produced I_2^- products. At 266 nm, however, I_2^- is only produced in an 80% yield. The above studies are in stark contrast to the gas phase work.

It is possible that a multiphoton rather than a single photon process creates I^-. Specifically, vibrationally cold I_2^- in its electronic ground state has a large dissociative cross section at 390 nm,[49,50] thereby allowing the possibility of a two-photon excitation to produce I^-:

$$I_3^- \xrightarrow{h\nu} I + I_2^-(^2\Sigma_u^+ ; v \approx 0) \xrightarrow{h\nu} I + I^- + I. \tag{2}$$
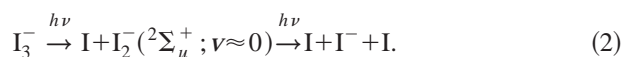
We previously reported an extensive power study varying the pump pulse intensity and monitoring the amount of I^- products formed.[21] A linear trend was found, implying that single photon excitation of I_3^- produces I^- products at 390 nm. The most likely reasons that Eq. (2) does not contribute significantly to I^- formation are because the majority of I_2^- products form after the FWHM of the pump pulse and because the I_2^- is also highly vibrationally excited, reducing its absorption cross section at 390 nm (see below).

Production of I^- can occur by either a two- or three-body mechanism:

$$I_3^- \xrightarrow{h\nu} I^- + I_2, \tag{3}$$

$$I_3^- \xrightarrow{h\nu} I^- + I + I. \tag{4}$$

The latter channel can be produced by a concerted three-body dissociation along the symmetric stretch of the potential, or, if the I_3^- first excited state correlates to a dissociative I_2^- potential (all of the excited states of I_2^- are dissociative or very weakly bound[41,51]), a sequential mechanism is also possible:

$$I_3^- \xrightarrow{h\nu} I + I_2^-(^2\Pi_{g,1/2}) \rightarrow I + I^- + I. \tag{5}$$
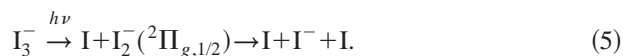
Distinguishing among these possible routes of I^- formation is not straightforward. However, the qualitative features of the time evolution of the $I(^2P_{3/2}) \leftarrow I^-$ transition suggest a mechanism following Eq. (4). This will be addressed after a discussion of the oscillatory features at intermediate energies.

C. Vibrationally excited, coherent I₂⁻

The photofragment mass spectra show that photolysis of I_3^- at 390 nm produces I_2^- in addition to I^-. The only features
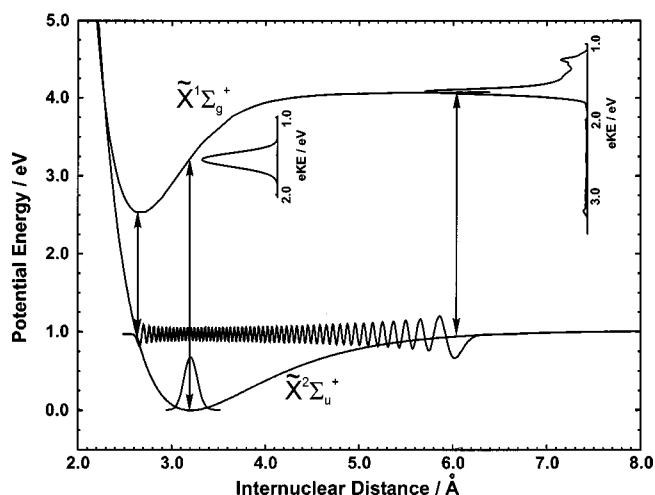
FIG. 9. Wave functions for $v=0$ and 110 on the I_2^- electronic ground state and their corresponding photoelectron spectra. The upper potential is the electronic ground state for I_2. Note that the inner turning point of the $v = 110$ eigenstate lies directly below the I_2 ground state, and the photoelectron spectrum reaches up to 3.2 eV.

so far not accounted for in the photoelectron spectrum are the broad features between 0.9 and 1.6 eV and the low intensity signal up to 3.2 eV. Neither feature appears in the photoelectron spectrum of vibrationally cold I_2^-,[42] in which photodetachment to the I_2 ground state yields a single feature centered at 1.6 eV and no intensity above 1.9 eV as shown in Fig. 9. However, a photoelectron signal from highly vibrationally excited I_2^- comes primarily from the inner and outer turning points of the anion wave function. Figure 9 shows the $I_2^-(v=110)$ wave function and the simulated photoelectron spectrum from this level. The spectrum consists of two well-separated features that straddle the $I_2^-(v=0)$ photoelectron spectrum; detachment from the inner turning point of the $v=110$ wave function produces electrons up to 3.2 eV, whereas detachment from the outer turning point yields a more intense feature between 1.2 and 1.8 eV. Note that the most intense peak around 1.6 eV is from the outermost part of the anion wave function. At slightly smaller internuclear distances, the vertical detachment energy increases slightly due to the greater curvature of the anion potential. Hence, photodetachment from the corresponding section of the anion wave function results in slower electrons.

We therefore attribute the remaining features in the experimental spectra to vibrationally excited I_2^-. The oscillations in these features, shown in Figs. 7 and 8, must then be due to coherent vibrational motion of the I_2^- photoproduct. Both the maximum observed eKE and the frequency of the vibrational coherences can be used to characterize the I_2^- vibrational distribution.

The maximum vibrational energy of the I_2^- can be directly obtained from the maximum eKE based on the following considerations. The $v=0$ wave function of I_2 has amplitude from 2.62 to 2.72 Å.[52] If the inner turning point of the

I_2^- vibrational wave function lies in this range, it will detach directly to $v=0$ of the I_2 ground state potential. Since the energy difference between $v=0$ of I_2^- is well known ($EA=2.52$ eV),[42] the vibrational energy can be determined. Thus, for 3.2 ± 0.1 eV electrons (Fig. 3, inset), the energy difference between the inner turning point of the I_2^- wave function and $v=0$ of the neutral state potential is 1.57 ± 0.1 eV using Eq. (1). This gives 0.95 ± 0.1 eV for the maximum vibrational energy. For the I_2^- Morse potential in Fig. 9,[42] photodetachment from all vibrational energy levels above 0.55 eV access the $I_2(v=0)$ state, so our result should be valid. We point out that this analysis directly yields the I_2^- vibrational energy; for the Morse potential in Fig. 9, the corresponding quantum number is 110, but the true quantum number is likely to differ because the Morse function is not very accurate so close to the dissociation limit.

The oscillatory I_2^- features, also in Fig. 7 and 8, provide further information on the I_2^- vibrational distribution. Because the I_3^- dissociation is initiated with a laser pulse shorter than a single period of product vibrational motion, the I_2^- photoproduct can be formed in a coherent superposition of vibrational levels spanning the nascent vibrational distribution. In the best case scenario, all of the frequencies associated with the product vibrational distribution will be in phase at short times and will lead to large amplitude wave packet oscillations which are detected in the FPES experiment. As time progresses, the frequencies will dephase from one another due to the anharmonicity of the potential. However, because of the collisionless nature of the gas phase environment, pure dephasing will not play a role and the I_2^- products should rephase at a much later time. Using the I_2^- ground state frequency and anharmonicity ($\omega_e=110$ cm^{-1} and $\omega_e\chi_e=0.37$ cm^{-1}),[42] the average vibrational state of the products can be determined along with the time at which rephasing might occur.

The 550 fs oscillations seen in the experiment correspond to an approximately 60 cm^{-1} energy difference which indicates a vibrational quantum number of $v=67$, or 0.70 eV of vibrational energy. From the anharmonicity, a predicted rephasing time of $\tau=45$ ps is calculated, in close agreement with experiment (Fig. 8). The number of states coherently populated, however, determines the dephasing time. If only three vibrational levels were populated, one would expect a dephasing time of $\tau/2$, which is much longer than the experimental dephasing time of ~4 ps. This indicates that a wide distribution of I_2^- states is populated. It is also consistent with a vibrational distribution having a maximum energy of 0.95 eV, determined from the maximum eKE, and an average energy of 0.70 eV, determined from the coherence frequency.

The accuracy of the average energy determined from the coherence frequency is limited by the Morse potential. A better method of determining the vibrational energy distribution is to measure the photofragment kinetic energy release from I_3^- photodissociation.[33] However, the coherences in our report can be directly compared to the solution experiments. In solution, I_2^- vibrational coherences were observed from photodissociated I_3^-,[12,17,19] with a period substantially shorter (350 fs) and the inferred average vibrational state ($\langle v\rangle$

$=12$) much lower than our results. This indicates that the ''nascent'' product distribution is quite different in solution than in the gas phase, a point discussed in Sec. V.

Although the traces in Fig. 7 show intensity beginning at 0 fs, it is unclear at what point this signal should be attributed to the I_2^- product. If we use as the criterion the start of the periodic oscillations, then the first maxima associated with the I_2^- product are at 400 fs (1.29 eV), 550 fs (1.41 eV), 700 fs (1.54 eV), and 850 fs (3.00 eV). At 1.41 eV, there is an earlier, smaller maximum at 100 fs. Since product coherence is generally expected to decay with time, the lower intensity of the earlier maximum suggests it is due to a transient I_3^- signal during the early stages of bond cleavage rather than to I_2^-. It also seems unlikely that I_2^- products would appear within 100 fs, since I^- is not fully formed until 600 fs. The transient I_3^- signal is probably the origin of the shoulder at 200 fs in the 3.00 eV slice as well.

D. Two-dimensional wave packet simulations

1. Potential energy surfaces and wave packet dynamics

We now characterize the I_3^- excited state potential energy surface on which dissociation occurs and investigate the mechanism responsible for the formation of atomic I^- products. In our previous report, one-dimensional (1D) wave-packet simulations using a Gaussian distribution of I_2^- vibrational states were carried out to ascertain the distribution of excited vibrational levels,[21] a procedure that is approximate at best. To model the photodissociation process more realistically and to determine the nature of the product coherences, we have performed two-dimensional (2D) wave packet simulations on a series of collinear London–Eyring–Polanyi–Sato (LEPS)[53] potential energy surfaces, and present the potential that best reproduces our I_2^- vibrational distribution. Although we do not model the full 2D photoelectron spectrum, we can simulate the spectrum once I_2^- is formed by projecting the 2D wave function onto the 1D wave function for I_2^- vibration. This LEPS potential also predicts that a substantial amount of three-body dissociation will occur via. Eq. (4) which we are also able to simulate in 1D and compare to the formation of the I^- feature at 1.7 eV.

This work was stimulated in part by the previous quantum simulations done by Banin et al.[13] in which a simple LEPS potential was used to model the excited potential energy surface. Like in their work, our simulation was carried out using a method based on the wave packet propagation techniques of Kosloff and Kosloff[54,55] and implemented by Bradforth et al.[56] It treats the dynamics along the two stretching coordinates exactly, and assumes that all nuclear motion takes place on a collinear potential energy surface.

Following Banin et al.,[13] we assume the ground state potential to be harmonic (Table I), the excited state potential to be a LEPS surface that correlates to ground state I_2^- products and an atomic iodine atom, and the pump pulse as being weak, coherent, and infinitely short. The iodine atomic product in their work, however, is assumed to be in its excited $^2P_{1/2}$ state since a pump frequency of 308 nm corresponds to excitation to the blue band in the I_3^- absorption spectrum. In

TABLE I. Parameters for the 1D and 2D potentials.

Ground state potential surface for I_3^-

$$V_g(Q_1,Q_3) = \tfrac{1}{2}\mu_1\omega_1^2(Q_1-Q_{eq})^2 + \tfrac{1}{2}\mu_2\omega_2^2(Q_3-Q_{eq})^2$$

$\omega_1{}^a = 112\text{ cm}^{-1}, \quad \omega_2{}^b = 145\text{ cm}^{-1}, \quad Q_{eq} = 5.358\text{ Å}, \quad \mu_1 = 63.5\text{ amu}, \quad \mu_3 = 21.2\text{ amu}$

Excited state potential surface for I_3^-

$$V_e(r_{ab},r_{bc},r_{ac}) = \Delta E_0 + Q_{ab} + Q_{bc} + Q_{ca} - (J_{ab}^2 + J_{bc}^2 + J_{ca}^2 - J_{ab}J_{bc} - J_{bc}J_{ca} - J_{ca}J_{ab})^{1/2}$$

$$Q_{\alpha\beta} = \frac{[(1+S_{\alpha\beta})E(r_{\alpha\beta})^1 + (1-S_{\alpha\beta})^3 E(r_{\alpha\beta})]}{2(1+S_{\alpha\beta})}, \quad {}^1E(r_{\alpha\beta}) = {}^1D[1-e^{-1\beta(r_{\alpha\beta}-{}^1r_{eq})}]^2 - {}^1D$$

$$J_{\alpha\beta} = \frac{[(1+S_{\alpha\beta})^1 E(r_{\alpha\beta}) - (1-S_{\alpha\beta})^3 E(r_{\alpha\beta})]}{2(1+S_{\alpha\beta})}, \quad {}^3E(r_{\alpha\beta}) = [{}^3D(1+e^{-3\beta(r_{\alpha\beta}-{}^3r_{eq})})^2 - {}^3D]/2$$

${}^1r_{eq} = 3.205\text{ Å}, \; {}^1D = 1.014\text{ eV}, \; {}^1\beta = 1.181\text{ Å}^{-1}, \; S_{ab} = S_{bc} = 0.50$

${}^3r_{eq} = 2.983\text{ Å}, \; {}^3D = 1.010\text{ eV}, \; {}^3\beta = 1.000\text{ Å}^{-1}, \; S_{ca} = 0.00$

$\Delta E_0 = 2.890\text{ eV}$

1D potentials for the symmetric stretch of neutral I_3

$$\begin{aligned} V_n(r) &= \Delta E_0 + 2D_e^n\exp[-\beta^n(r-r_e^n)] + D_e^n\exp[-2\beta^n(r-r_e^n)] \equiv \nu_1(r), \quad 0 < r \leqslant 7\text{ Å} \\ &= sf_1(r)\nu_1(r) + [1-sf_1(r)]\nu_2(r), \quad 7\text{ Å} < r \leqslant 11\text{ Å} \\ &= \Delta E_0 + 2D_e\exp[-\beta(r-r_e)] + D_e\exp[-2\beta(r-r_e)] \equiv \nu_2(r), \quad 11\text{ Å} < r \leqslant r_\infty \end{aligned}$$

$$sf_n(r) = \frac{1}{2}\left(\cos\frac{\pi(r-r_n)}{r_{n+1}-r_n} + 1\right)$$

$r_e = 5.66\text{ Å}, \; D_e = 1.47\text{ eV}, \; \beta = 0.53\text{ Å}^{-1}, \; \Delta E_0 = 5.95\text{ eV}$

V_1: $r_e^1 = 5.10\text{ Å}, \; D_e^1 = 1.70\text{ eV}, \; \beta^1 = 0.38\text{ Å}^{-1}$

V_2: $r_e^2 = 5.66\text{ Å}, \; D_e^2 = 1.47\text{ eV}, \; \beta^2 = 0.45\text{ Å}^{-1}$

V_3: $r_e^3 = 6.10\text{ Å}, \; D_e^3 = 1.27\text{ eV}, \; \beta^3 = 0.52\text{ Å}^{-1}$

[a]Symmetric stretch frequency taken from this article, Sec. IV A.
[b]Antisymmetric stretch reported in Ref. 29.

our experiment, excitation at 390 nm corresponds to excitation into the lower I_3^- absorption band, which predominantly results in $I(^2P_{3/2})$ products.[33] This also means the energy available for bond dissociation differs between the two experiments. Banin *et al.* determined the available energy to be ~0.4 eV above the three-body dissociation limit of $I^- + I(^2P_{3/2}) + I^*(^2P_{1/2})$,[13] based on an approximate value of 1.0 eV for the bond strength of I_3^-.[31] Since publication of their work a gas phase bond strength of 1.31 ± 0.06 eV has been reported,[20] showing the amount of available energy is actually much smaller. Using similar energetic arguments, the new I_3^- bond strength and the more recent bond strength for I_2^-,[42] ~0.3 eV of energy is estimated to be available for product dissociation at 390 nm to $I^- + I(^2P_{3/2}) + I(^2P_{3/2})$. With this in mind, the ground state geometry is adjusted so that a vertical transition to the excited state lies 0.3 eV above the three-body asymptote.

In an effort to understand the features required to produce vibrationally excited I_2^- products, we first ran simulations, using the methods described below, on the original Banin *et al.* excited state potential with the I_3^- ground state geometry adjusted so that the vertical transition energy was 0.3 eV above the three-body asymptote. We found that this surface yielded considerably less I_2^- vibrational excitation than was observed experimentally, and no I^- was produced. We then adjusted the Sato parameters on the excited state

surface to achieve better agreement with experiment. The original potential had a barrier of ~300 meV along the minimum energy path for the symmetric exchange reaction $I + I_2^- \rightarrow I_2^- + I$. Lowering the barrier resulted in more I_2^- vibrational excitation, but not until the barrier was eliminated in favor of a shallow well did the I_2^- vibrational distribution peak at vibrational energies comparable to our experiment. This modification also produced more I^- via three-body dissociation, as is shown below.

The final potential is shown in Fig. 10, along with snapshots of the wave packet evolving in 100 fs intervals, starting from its initial placement vertically above the ground state minimum. The potential is presented in mass weighted coordinates for the linear $I_A - I_B - I_C$ molecule with the *x* axis representing the distance from I_C to the center of mass of the departing $I_2^-(I_A - I_B)$ product. The *y* axis corresponds to the I_2^- bond length $R_{A,B}$. The parameters for the potentials are listed in Table I.

The initial motion is primarily along the symmetric stretch coordinate of the potential, consistent with the resonance Raman work.[29,30] Once the wave packet passes through the potential well (~100 fs) it begins spreading along the antisymmetric stretching coordinate. This broadening continues until the wave packet boundaries reach the repulsive walls in the I_2^- product valleys at around 400 fs. By this time, the wave packet spans the entire potential but still
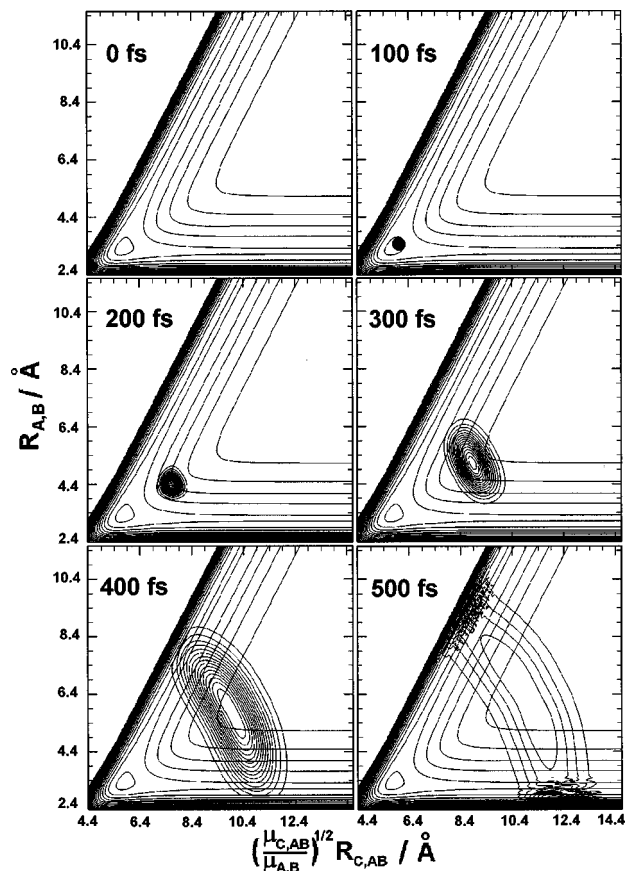
FIG. 10. Snapshots of the evolving wave packet on the 2D LEPS potential for the excited state of I_3^- from Table I. The potential is shown in mass-weighted coordinates for the linear $I_A - I_B - I_C$ molecule. $R_{C,AB}$ is the distance between I_C and the center of mass of the I_2^- fragment $(I_A - I_B)$, and $R_{A,B}$ is the I_2^- bond length. The contours for the potential are in ~ 200 meV steps and the contours for the wave packet represent a 10% change in $|\Psi|^2$. At 500 fs, significant intensity remains along the symmetric stretching coordinate.

has significant intensity along the symmetric stretching coordinate, in contrast to the surface reported by Banin et al.[13] By 500 fs the wave packet is entirely out of the transition state region, and continues to expand as the products move apart. The simulations in Fig. 10 show similar features to those of Banin et al., but the wave packet progresses further along the symmetric stretch coordinate before spreading on our surface, a direct consequence of the shallow well in the transition state region which accelerates the wave packet along the symmetric stretch coordinate.

By 500 fs, the portion of the wave packet residing in the upper and lower I_2^- valleys will form $I + I_2^-$ and $I_2^- + I$ products, respectively, while the remaining portion of the wave packet will form $I^- + I + I$ via Eq. (4). Assuming that there is equal probability for dissociating to $I + I_2^-$ or $I_2^- + I$ products, and that the dividing line between lower valley products and three-body dissociation products occurs at $R_{A,B} = 5.5$ Å, integration of the lower valley gives a 27% probability for three-body dissociation at 500 fs. To insure that further motion did not significantly decrease the three-body yield, the wave packet was allowed to evolve for an additional 150 fs, and the three-body dissociation probability was again determined to be 27%.
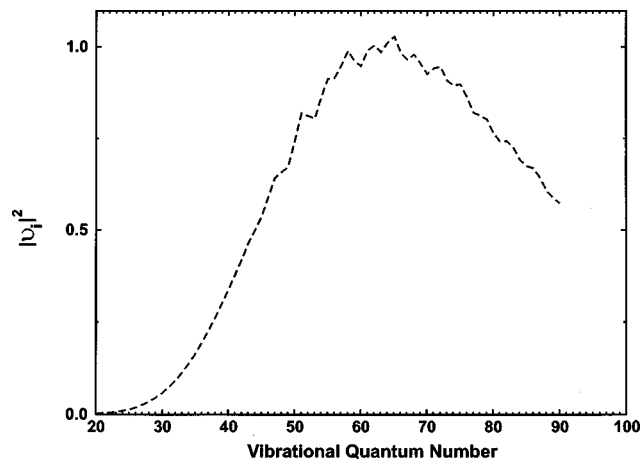
FIG. 11. Vibrational energy distribution [Eq. (6)] for the 2D wave packet at 500 fs.

2. I_2^- vibrational distribution and dynamics

At times $\geqslant 500$ fs, the wave packet has essentially reached the asymptotic region of the potential energy surface, so that slices through the upper and lower valleys perpendicular to the minimum energy path yield the Morse function for the I_2^- ground state. In the lower valley, the wave packet can therefore be decomposed into vibrational and translational eigenstates according to

$$\Psi(x,y) = \sum_{n,i} c_{n,i} \phi_n(x) \chi_i(y), \qquad (6)$$

where $\chi_i(y)$ are the Morse oscillator wave functions for the I_2^- ground state, and $\phi_n(x)$ are 1D free particle waves.[57] On this basis x and y are perpendicular and parallel, respectively, to the minimum energy path. Only intensity at internuclear distances smaller than $R_{A,B} = 5.5$ Å is decomposed in this manner since the basis only applies to those products correlating to $I_2^- + I$. Using the coefficients determined, the vibrational energy distribution is determined by first squaring and then summing (over n) the coefficients along the translational coordinate, and the results are plotted in Fig. 11. The maximum occurs at $v = 65$ with a FWHM of 50 vibrational states. It is also asymmetric, with a tail that reaches to at least $v = 120$, in agreement with our analysis in Sec. IV C.

At early delay times, 2D calculations are required to simulate the photoelectron spectrum arising from detachment of dissociating I_3^-. However, at delay times longer than 500 fs, the portion of the photoelectron spectra due to detachment of I_2^- in the lower valley only depends on the y-axis motion of the wave packet. This allows the spectra to be simulated using our previously developed 1D simulation code.[58] Using the above coefficients, a time-dependent 1D wave function was generated using the wave function at 500 fs as a starting point. Photoelectron spectra were then calculated from 500 to 4000 fs for detachment to the $\tilde{X}\,^1\Sigma_g^+$, $\tilde{A}'\,^3\Pi_{2u}$, and $\tilde{A}\,^3\Pi_{1u}$ states of neutral I_2.[52,59,60] The results were convoluted to match our energy resolution and energy slices were taken for comparison with experiment (Fig. 7, dashed line).

In agreement with experiment, the simulations produce 550 fs oscillations that rapidly dephase by 4 ps and reflect
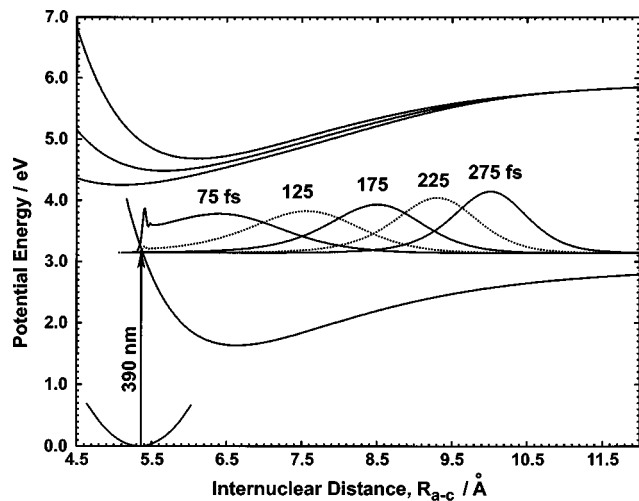
FIG. 12. 1D potentials representing the symmetric stretching coordinate for the I_3^- anion ground, excited, and lowest three neutral I_3 states. The parameters are given in Table I. Wave packets created by the 1D simulation described in Sec. IV D are also displayed.

FIG. 13. Simulated 1D FPES spectra of the atomic $I(^2P_{3/2}) \leftarrow I^-$ feature at 1.7 eV. The three peaks at 75 fs arise from detachment to the three neutral states and the transformation from a broad spectrum to the atomic feature occurs starting at around 175 fs.

the same energy dependent phase shift. The first maximum is due to reflection at the inner turning point and occurs at 650 fs at eKE$=3.00$ eV. Reflection from the outer turning point is observed 275 fs later in the slice at 1.54 eV. Results at 1.29 and 1.41 eV reflect wave packet motion in between these two limits (see Fig. 9 and Sec. III C).

However, the maxima in the simulated energy slices fall directly between the maxima in the experimental slices. For example, at 1.29 eV, the first two experimental maxima occur at 400 and 1000 fs, whereas the first simulated maximum is at 700 fs. As mentioned above, this simulated maximum is associated with wave packet amplitude near the outer turning point of the I_2^- potential. In a 2D simulation of the photoelectron spectrum, we would expect an earlier maximum at 1.29 eV around 200–300 fs associated with wave packet bifurcation into the product valleys, because the wave packet motion along the symmetric stretch coordinate slows down significantly in the region where bifurcation begins (see Fig. 10). It is therefore reasonable to assign the first two experimental maxima at 400 and 1000 fs to wave packet bifurcation and the first bond compression of the newly formed I_2^-. Hence, although there is significant agreement between the experimental and simulated energy slices, it appears that the maxima in the simulated energy slices occur too early.

3. I^- channel

We can also explore production of I^- on this surface. If I^- production occurs via concerted three-body dissociation, detachment of the wave packet along the symmetric stretching coordinate of I_3^- should give rise to the atomic I^- features in Figs. 3 and 6. It should therefore be possible to reproduce the main trends in the I^- features by performing 1D simulations of wave packet motion along the symmetric stretch coordinate of the potential in Fig. 10.

Shown in Fig. 12 are cuts along the symmetric stretching coordinate of the ground and excited state I_3^- potentials. Potentials for I_3 are also needed. These are represented by
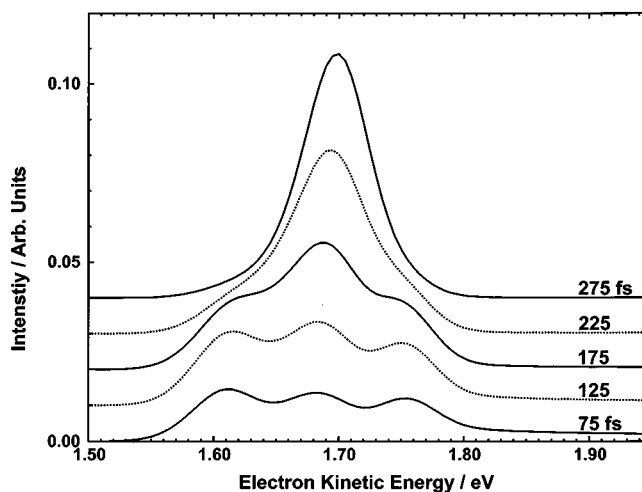
Morse–Morse-switching-function potentials (Table I) with vertical electron affinities of 4.25, 4.52, and 3.32 eV that match those measured for the ground and first two excited states of neutral I_3 (Sec. III A). Using the same initial wave function in the 1D simulation as was used along the symmetric stretch coordinate of the 2D simulations, the wave packet is coupled to the excited anion state by a pump pulse where it is propagated, the time-dependent photoelectron spectrum is calculated using a technique described previously,[58] and the results are convoluted with an instrument response function. To more realistically model the spectra the pump pulse was given a FWHM of 90 fs. Figure 13 shows the calculated photoelectron spectra at delay times of 75, 125, 175, 225, and 275 fs, and the wave packets that correspond to these delay times are shown in Fig. 12.

In the simulated spectra, formation of the I^- feature at 1.7 eV occurs in two steps, in agreement with experiment (Figs. 3 and 6). At 75 and 125 fs a broad distribution of energies is formed ranging from 1.55 to 1.80 eV with three features at 1.61, 1.67, and 1.76 eV. At these times the wave packet resides primarily at internuclear distances near the potential minimum along the symmetric stretch coordinate (see Fig. 12), and the three small features arise from detachment to the three neutral states. At 175 fs the simulated spectrum has leveled and begun to narrow, at which time the wave packet is approximately halfway out of the potential minimum. At this internuclear distance ($\sim$8.5 Å), the anion and neutral potentials are nearly parallel. By 275 fs the wave packet has largely left the potential minimum and the photoelectron spectrum is dominated by a single atomic peak at 1.7 eV. Thus, the two-step trend in the photoelectron spectrum corresponds to the wave packet traversing the potential minimum along the symmetric stretching coordinate of the 2D potential energy surface, and the narrowing of the $I(^2P_{3/2}) \leftarrow I^-$ feature is a consequence of the wave packet

climbing out of the potential well and leaving the transition state region, by which point the three I$_3$ surfaces have almost converged. Therefore, in the simulations, bond cleavage to I$^-$+I+I occurs between 175 and 275 fs when the I($^2P_{3/2}$)←I$^-$ feature narrows in width.

The qualitative agreement between the simulation and experiment leads us to believe that I$^-$ is being formed by three-body dissociation via Eq. (4). However, the narrowing of the I($^2P_{3/2}$)←I$^-$ feature at 1.7 eV experimentally occurs at 300 fs, not at 175 fs as in the simulation, and suggests that the simulated wave packet leaves the transition state region too quickly. This is consistent with our conclusions modeling the I$_2^-$ coherences; the simulated I$^-$ and I$_2^-$ products form too quickly with this LEPS potential. A surface with a potential well that extends to larger internuclear distances may decrease the discrepancy in both cases, or the slope of the excited state potential in the Franck–Condon region may be too steep, imparting too much momentum to the wave packet. We also must consider the limitations inherent in explaining the dynamics with a collinear rather than three-dimensional potential energy surface. In any case, comparison of the simulations to experiment indicates that the bond cleavage to I$^-$+I+I occurs between 300 and 600 fs.

V. DISCUSSION AND COMPARISON OF GAS AND SOLUTION PHASE DYNAMICS

There are significant differences between the gas phase and solution photodissociation dynamics of I$_3^-$. In the I$_3^-$/EtOH experiments involving excitation to the lower electronic state, oscillations from I$_2^-$ products are first resolved at approximately 500 fs with a frequency of 103 cm^{-1}.[17] This corresponds to $\langle v \rangle = 12(0.13\,\mathrm{eV})$,[42] a considerably colder population than seen in the gas phase. In addition, no I$^-$ product was seen in the solution experiments at 400 nm, in contrast to the significant amount of I$^-$ seen in the gas phase. Based on the simulations in Sec. IV, we understand what type of early time ($<$500 fs) dynamics lead to the observed gas phase results. We now consider how these dynamics are modified in solution.

Four effects unique to the experiments in solution are (1) symmetry breaking of the I$_3^-$ due to its interaction with the polar solvent, (2) solvent friction effects on the dissociation dynamics in the transition state region, (3) vibrational relaxation of the I$_2^-$ products, and (4) solvent induced dephasing. It is useful to distinguish these effects by the time interval over which they are important. Symmetry breaking, in which the $D_{\infty h}$ symmetry of the anion is lowered to $C_{\infty v}$, represents an initial-state effect whereby the anion is distorted before any laser fields are applied. Solvent friction in the transition state region is relevant to the time interval just after excitation, when the dissociating wave packet is in transit between the Franck–Condon region and the I$_2^-$ product valleys. Finally, solvent induced dephasing occurs throughout the reaction while vibrational relaxation is relevant once the I$_2^-$ products are formed.

The observation by Johnson and Myers[29,30] of antisymmetric stretch excitation in the resonance Raman spectrum of I$_3^-$/EtOH provides strong evidence of symmetry breaking. In

addition, Geshgoren et al.[15] performed femtosecond dissociation experiments on I$_3^-$ in CH$_3$CN, a less polar solvent than ethanol, and found that the I$_2^-$ product coherences were less pronounced. This was attributed to a more rapid and coherent entry into the I$_2^-$ product valley induced by broken symmetry of the I$_3^-$ anion in the more polar solvent. This interpretation is consistent with the wave packet simulations in Fig. 10; if the initial wave packet did not lie along the symmetric stretch coordinate, one would expect less motion along the symmetric stretch coordinate and earlier localization in one of the product valleys. As a result, the I$_2^-$ vibrational population would be colder and less I$^-$ would be produced, consistent with the differences between the gas phase and solution experiments. Symmetry breaking of I$_3^-$ has also been modeled theoretically[61,62] and similar effects on the I$_2^-$ vibrational distribution are expected in the photodissociation of I$_3^-$ with antisymmetric stretch excitation.[57]

Solvent friction effects can also play a role consistent with the differences in the gas phase and solution experiments. Suppose that in solution the initial wave packet in Fig. 10 does lie along the symmetric stretch coordinate. One would then expect interactions with the solvent to impede the motion of the wave packet along this coordinate, leading to bifurcation of the wave packet at smaller internuclear distances than in the absence of solvent. This, like symmetry breaking, would result in a colder I$_2^-$ distribution and reduced I$^-$ formation.

Vibrational relaxation of the I$_2^-$ products may account for some of the discrepancy between the gas phase and solution experiments. The relaxation rate of I$_2^-$ is known to be strongly vibrational state dependent. In the I$_3^-$/EtOH experiments, an estimated 0.17 eV of vibrational energy is lost within 7 ps although 0.13 eV of this energy is dissipated during the first 1.5 ps.[17] In experiments monitoring the recombination of photodissociated I$_2^-$ in ethanol, $\sim$0.75 eV of vibrational energy is dissipated in the first 0.3 ps while the remaining 0.25 eV of vibrational energy takes $\sim$10 ps to dissipate.[63,64] Hence, extremely fast relaxation rates for vibrational levels above $v=30$ are expected,[64] and relaxation of these highly excited levels may have already occurred by 500 fs, the earliest time at which clear I$_2^-$ coherences are seen in solution. Solvent induced dephasing accounts for a portion of the coherence loss of I$_3^-$ in solution although this does not affect the vibrational distribution.[13,17]

It is likely that symmetry breaking as well as solvent friction and vibrational relaxation effects contribute to the differences between the I$_3^-$ experiments. We note that similar but smaller differences are seen in HgI$_2$ photodissociation in the gas phase and in solution. The gas phase reaction produces coherent HgI in approximately $\langle v \rangle = 29$ (0.31 eV of vibrational energy).[4] In EtOH solution, one finds $\langle v \rangle = 15$ for HgI at 500 fs, corresponding to 0.21 eV of vibrational energy.[7] Symmetry breaking is unlikely to occur in HgI$_2$ because of its weaker interaction with the solvent molecules, so in this case solvent friction and vibrational relaxation are the likely causes of the lower vibrational energy at the earliest observation times.

A possible means of gaining further insight into differences between the I$_3^-$ experiments is to perform experiments

on clustered I_3^-. For example, in the binary cluster I_3^-(EtOH), the interaction between the I_3^- and EtOH could easily be strong enough to induce distortion in the I_3^-, but the presence of only a single ''solvent'' molecule is unlikely to perturb the outgoing I_2^- photoproduct significantly. Hence, a significantly colder I_2^- vibrational distribution in this case would point to symmetry breaking as the primary culprit. Experiments of this type will be carried out in the near future in our laboratory.

Regardless of the origin of the differences between the gas phase and solution experiments, the results presented here emphasize the importance of studying reactions in both environments. The scope and significance of the solvent effects in I_3^- photodissociation cannot be appreciated without comparison to the gas phase results. By the time I_2^- photoproducts can be unambiguously identified in solution, they are already significantly colder than the gas phase photoproducts. The potential energy surface constructed in this work, although approximate, provides a foundation for a better understanding of the reaction dynamics in solution.

VI. CONCLUSIONS

We report the first study on the gas phase photodissociation dynamics of I_3^-. The experimental method, femtosecond photoelectron spectroscopy, allows us to simultaneously observe depletion of the I_3^- reactant and formation of the ionic photoproducts I_2^- and I^-. We find that I^- and I_2^- are produced in approximately equal yield, in contrast to photodissociation experiments at a similar wavelength in solution where only I_2^- was observed.

The femtosecond photoelectron spectra reveal vibrational coherences in the I_3^- reactant induced by resonant impulsive stimulated Raman scattering, from which we obtain a symmetric stretch frequency of 112 cm^{-1} for the I_3^- ground state. Starting around 400 fs, coherent nuclear motion of the I_2^- products is also observed which exhibits rapid dephasing due to the anharmonicity of the potential followed by rephasing at much longer times. The oscillation period of these coherences yield an average $\langle \nu \rangle = 67$, a much higher result than obtained in ethanol solution ($\langle \nu \rangle = 12$).

Two-dimensional wave packet simulations on a collinear I_3^- excited state surface yielded further insight into the dissociation dynamics. A surface was constructed that yielded the appropriate I_2^- vibrational distribution and also resulted in significant I^- production. A comparison of simulations with the time dependence of the I^- photoelectron signal indicates the I^- is produced by concerted three-body dissociation. The excited state surface is clearly approximate since both channels are produced too quickly in the simulations, but it should serve a useful starting point for future analysis of this system.

A comparison of the gas phase and solution dynamics indicates that the differences are most likely to arise from symmetry breaking effects of the solvent on the I_3^- chromophore and to solvent effects in the first several hundred femtoseconds after photodissociation. In comparison with the HgI$_2$ system, I_3^- photodissociation provides a more extreme example of the solvent's ability to alter chemical dynamics. Future work will focus on experiments monitoring the product yield and degree of coherence on the stepwise solvation of I_3^- in size-selected clusters. This should yield information on the role of solvent in symmetry breaking and energy partitioning.

[1] M. L. Chabinyc, S. L. Craig, C. K. Regan, and J. I. Brauman, Science **279**, 1882 (1998).
[2] M. Volk, S. Gnanakaran, E. Gooding, Y. Kholodenko, N. Pugliano, and R. M. Hochstrasser, J. Phys. Chem. A **101**, 638 (1997).
[3] R. M. Bowman, M. Dantus, and A. H. Zewail, Chem. Phys. Lett. **156**, 131 (1989).
[4] M. Dantus, R. M. Bowman, M. Gruebele, and A. H. Zewail, J. Chem. Phys. **91**, 7437 (1989).
[5] M. Dantus, R. M. Bowman, J. S. Baskin, and A. H. Zewail, Chem. Phys. Lett. **159**, 406 (1989).
[6] M. Gruebele, G. Roberts, and A. H. Zewail, Philos. Trans. R. Soc. London, Ser. A **332**, 223 (1990).
[7] N. Pugliano, D. K. Palit, A. Z. Szarka, and R. M. Hochstrasser, J. Chem. Phys. **99**, 7273 (1993).
[8] N. Pugliano, A. Z. Szarka, S. Gnanakaran, M. Triechel, and R. M. Hochstrasser, J. Chem. Phys. **103**, 6498 (1995).
[9] N. Pugliano, A. Z. Szarka, and R. M. Hochstrasser, J. Chem. Phys. **104**, 5062 (1996).
[10] S. Gnanakaran, M. Lim, N. Pugliano, M. Volk, and R. M. Hochstrasser, J. Phys.: Condens. Matter **8**, 9201 (1996).
[11] U. Banin, A. Waldman, and S. Ruhman, J. Chem. Phys. **96**, 2416 (1992).
[12] U. Banin and S. Ruhman, J. Chem. Phys. **98**, 4391 (1993).
[13] U. Banin, R. Kosloff, and S. Ruhman, Isr. J. Chem. **33**, 141 (1993).
[14] U. Banin, R. Kosloff, and S. Ruhman, Chem. Phys. **183**, 289 (1994).
[15] E. Gershgoren, E. Gordon, and S. Ruhman, J. Chem. Phys. **106**, 4806 (1997).
[16] E. Gershgoren, U. Banin, and S. Ruhman, J. Phys. Chem. A **102**, 9 (1998).
[17] T. Kühne and P. Vöhringer, J. Chem. Phys. **105**, 10788 (1996).
[18] T. Kühne and P. Vöhringer, J. Phys. Chem. A **102**, 4177 (1998).
[19] T. Kühne, R. Küster, and P. Vöhringer, Chem. Phys. **233**, 161 (1998).
[20] K. Do, T. P. Klein, C. A. Pommerening, and L. S. Sunderlin, J. Am. Soc. Mass Spectrom. **8**, 688 (1997).
[21] M. T. Zanni, B. J. Greenblatt, A. V. Davis, and D. M. Neumark, Proc. SPIE **3271**, 196 (1998).
[22] R. E. Buckles, J. P. Yuk, and A. I. Popov, J. Am. Chem. Soc. **74**, 4379 (1952).
[23] W. Gabes and D. J. Stufkens, Spectrochim. Acta A **30**, 1835 (1974).
[24] M. Mizuno, J. Tanaka, and I. Harada, J. Phys. Chem. **85**, 1789 (1981).
[25] T. Okada and J. Hata, Mol. Phys. **43**, 1151 (1981).
[26] K. Kaya, N. Mikami, Y. Udagawa, and T. Ito, Chem. Phys. Lett. **16**, 151 (1972).
[27] W. Kiefer and H. J. Bernstein, Chem. Phys. Lett. **16**, 5 (1972).
[28] H. Isci and W. R. Mason, Inorg. Chem. **24**, 271 (1985).
[29] A. E. Johnson and A. B. Myers, J. Chem. Phys. **102**, 3519 (1995).
[30] A. E. Johnson and A. B. Myers, J. Phys. Chem. **100**, 7778 (1996).
[31] L. E. Topol, Inorg. Chem. **10**, 736 (1971).

[32] T. R. Taylor, K. Asmis, M. T. Zanni, and D. M. Neumark, J. Chem. Phys. **110**, 7607 (1999).

[33] H. Choi, R. T. Bise, A. A. Hoops, and D. M. Neumark, J. Chem. Phys. (unpublished).

[34] B. J. Greenblatt, M. T. Zanni, and D. M. Neumark, Chem. Phys. Lett. **258**, 523 (1996).

[35] B. J. Greenblatt, M. T. Zanni, and D. M. Neumark, Faraday Discuss. **108**, 101 (1998).

[36] O. Cheshnovsky, S. H. Yang, C. L. Pettiette, M. J. Craycraft, and R. E. Smalley, Rev. Sci. Instrum. **58**, 2131 (1987).

[37] H. Handschuh, G. Gantefor, and W. Eberhardt, Rev. Sci. Instrum. **66**, 3838 (1995).

[38] L.-S. Wang, H.-S. Cheng, and J. Fan, J. Chem. Phys. **102**, 9480 (1995).

[39] M. D. Davidson, B. Broers, H. G. Muller, and H. B. van Linden van den Heuvell, J. Phys. B **25**, 3093 (1992).

[40] B. J. Greenblatt, M. T. Zanni, and D. M. Neumark, Science **276**, 1675 (1997).

[41] M. T. Zanni, V. S. Batista, B. J. Greenblatt, W. H. Miller, and D. M. Neumark, J. Chem. Phys. **110**, 3748 (1998).

[42] M. T. Zanni, T. R. Taylor, B. J. Greenblatt, B. Soep, and D. M. Neumark, J. Chem. Phys. **107**, 7613 (1997).

[43] A. Mokhtari and J. Chesnoy, Europhys. Lett. **5**, 523 (1988).

[44] J. Chesnoy and A. Mokhtari, Phys. Rev. A **38**, 3566 (1988).

[45] S. L. Dexheimer, Q. Wang, L. A. Peteanu, W. T. Pollard, R. A. Mathies, and C. V. Shank, Chem. Phys. Lett. **188**, 61 (1992).

[46] W. T. Pollard and R. A. Mathies, Annu. Rev. Phys. Chem. **43**, 497 (1992).

[47] U. Banin, A. Bartana, S. Ruhman, and R. Kosloff, J. Chem. Phys. **101**, 8461 (1994).

[48] W. Gabes and H. Gerding, J. Mol. Struct. **14**, 267 (1972).

[49] C. J. Delbecq, W. Hayes, and P. H. Yuster, Phys. Rev. **121**, 1043 (1961).

[50] T. Shida, Y. Takahashi, and H. Hatano, Chem. Phys. Lett. **33**, 491 (1975).

[51] E. C. M. Chen and W. E. Wentworth, J. Phys. Chem. **89**, 4099 (1985).

[52] F. Martin, R. Bacis, S. Churassy, and J. Verges, J. Mol. Spectrosc. **116**, 71 (1986).

[53] S. Sato, J. Chem. Phys. **23**, 592 (1955).

[54] R. Kosloff and D. Kosloff, J. Chem. Phys. **79**, 1823 (1983).

[55] D. Kosloff and R. Kosloff, J. Comput. Phys. **52**, 35 (1988).

[56] S. E. Bradforth, A. Weaver, D. W. Arnold, R. B. Metz, and D. M. Neumark, J. Chem. Phys. **92**, 7205 (1990).

[57] G. Ashkenazi, R. Kosloff, S. Ruhman, and H. Tal-Ezer, J. Chem. Phys. **103**, 10005 (1995).

[58] V. S. Batista, M. T. Zanni, B. J. Greenblatt, D. M. Neumark, and W. H. Miller, J. Chem. Phys. **110**, 3736 (1998).

[59] D. R. T. Appadoo, R. J. Leroy, P. F. Bernath, S. Gerstenkorn, P. Luc, J. Verges, J. Sinzelle, J. Chevillard, and Y. Daignaux, J. Chem. Phys. **104**, 903 (1996).

[60] X. N. Zheng, S. L. Fei, M. C. Heaven, and J. Tellinghuisen, J. Chem. Phys. **96**, 4877 (1992).

[61] H. Sato, F. Hirata, and A. B. Myers, J. Phys. Chem. A **102**, 2065 (1998).

[62] R. M. Lynden-Bell, R. Kosloff, S. Ruhman, D. Danovich, and J. Vala, J. Chem. Phys. **109**, 9928 (1998).

[63] D. A. V. Kliner, J. C. Alfano, and P. F. Barbara, J. Chem. Phys. **98**, 5375 (1993).

[64] P. K. Walhout, J. C. Alfano, K. A. M. Thakur, and P. F. Barbara, J. Phys. Chem. **99**, 7568 (1995).